

## Effective mass in bilayer graphene at low carrier densities: The role of potential disorder and electron-electron interaction

J. Li,<sup>1</sup> L. Z. Tan,<sup>2,3,\*</sup> K. Zou,<sup>1,†</sup> A. A. Stabile,<sup>1</sup> D. J. Seiwel,<sup>1</sup> K. Watanabe,<sup>4</sup> T. Taniguchi,<sup>4</sup> Steven G. Louie,<sup>2,3,‡</sup> and J. Zhu<sup>1,5,§</sup>

<sup>1</sup>*Department of Physics, The Pennsylvania State University, University Park, Pennsylvania 16802, USA*

<sup>2</sup>*Department of Physics, University of California at Berkeley, Berkeley, California 94720, USA*

<sup>3</sup>*Materials Sciences Division, Lawrence Berkeley National Laboratory, Berkeley, California 94720, USA*

<sup>4</sup>*National Institute for Material Science, 1-1 Namiki, Tsukuba 305-0044, Japan*

<sup>5</sup>*Center for 2-Dimensional and Layered Materials, The Pennsylvania State University, University Park, Pennsylvania 16802, USA*

(Received 6 July 2016; revised manuscript received 2 September 2016; published 25 October 2016)

In a two-dimensional electron gas, the electron-electron interaction generally becomes stronger at lower carrier densities and renormalizes the Fermi-liquid parameters, such as the effective mass of carriers. We combine experiment and theory to study the effective masses of electrons and holes  $m_e^*$  and  $m_h^*$  in bilayer graphene in the low carrier density regime on the order of  $1 \times 10^{11} \text{ cm}^{-2}$ . Measurements use temperature-dependent low-field Shubnikov-de Haas oscillations observed in high-mobility hexagonal boron nitride supported samples. We find that while  $m_e^*$  follows a tight-binding description in the whole density range,  $m_h^*$  starts to drop rapidly below the tight-binding description at a carrier density of  $n = 6 \times 10^{11} \text{ cm}^{-2}$  and exhibits a strong suppression of 30% when  $n$  reaches  $2 \times 10^{11} \text{ cm}^{-2}$ . Contributions from the electron-electron interaction alone, evaluated using several different approximations, cannot explain the experimental trend. Instead, the effect of the potential fluctuation and the resulting electron-hole puddles play a crucial role. Calculations including both the electron-electron interaction and disorder effects explain the experimental data qualitatively and quantitatively. This Rapid Communication reveals an unusual disorder effect unique to two-dimensional semimetallic systems.

DOI: [10.1103/PhysRevB.94.161406](https://doi.org/10.1103/PhysRevB.94.161406)

Bilayer graphene is a unique two-dimensional electron gas (2DEG) system with unusual electronic properties [1]. At high carrier densities, its hyperbolic bands are well described by a four-band Hamiltonian [2,3] given by the tight-binding (TB) description [4] where the hopping parameters are determined by experiments or first-principles calculations [5–10]. Close to the charge neutrality point (CNP), bilayer graphene exhibits fascinating electron-electron ( $e-e$ ) interaction-driven ground states [11–15]. A natural question arises: How does the density of states of bilayer graphene at the Fermi energy evolve as carrier density  $n$  decreases continuously? The study of the effective carrier mass  $m^*$  is a powerful tool to probe this evolution. Indeed, in conventional 2DEGs, increasing  $e-e$  interaction leads to a substantial increase in  $m^*$  at low carrier densities, long before predicated many-body instabilities [16–21]. Such studies provide valuable input to advance many-body calculations [22]. In monolayer and bilayer graphene, the close proximity of the conduction and valence bands and their pseudospin characters play a significant role in the screening of the Coulomb interaction. This has consequences for the dispersions of the elementary excitations and the transport properties of these systems [23–26]. In monolayer graphene, both calculations [27] and measurements of  $m^*$  [28,29] report

strong enhancement of the Fermi velocity  $v_F$  at low carrier densities. The situation in bilayer graphene is much less clear. Existing theoretical predictions vary greatly on the sign and magnitude of the interaction correction to  $m^*$  [30–35] whereas measurements have been lacking.

In our earlier work [10], we reported on the measurements of  $m^*$  in bilayer graphene in the density regime on the order of  $1 \times 10^{12} \text{ cm}^{-2}$ . A TB description was found to work well, the hopping parameters of which were accurately extracted from data. As the previous samples rested on oxides, Coulomb potential disorder (field effect mobility  $\mu_{FE} \sim$  a few thousand  $\text{cm}^2 \text{ V}^{-1} \text{ s}^{-1}$ , and disorder energy  $\delta E$  of a few tens of meV [36,37]) prevented measurements at lower densities. In our current hexagonal boron nitride (h-BN) supported samples,  $\mu_{FE}$  reaches  $30\,000 \text{ cm}^2 \text{ V}^{-1} \text{ s}^{-1}$ , which allows for the precise determination of  $m^*$  down to  $n = 2 \times 10^{11} \text{ cm}^{-2}$  for both electrons and holes. Following the conventional definition of the interaction parameter  $r_s = U/E_F$ , where  $U$  is the Coulomb interaction energy  $e^2\sqrt{n\pi}/(4\pi\epsilon_0\epsilon)$  and  $E_F$  is the Fermi energy, we estimate  $r_s$  to be  $7.5/\sqrt{n}$  (in units of  $10^{11} \text{ cm}^{-2}$ ) using  $m^* = 0.033 m_e$ , which is the average value of the measured electron and hole masses near  $1 \times 10^{12} \text{ cm}^{-2}$  in Ref. [10]. In our presently studied carrier density regime ( $2-12 \times 10^{11} \text{ cm}^{-2}$ ),  $r_s$  ranges from 2.2 to 5.3, which is comparable to the range studied in GaAs electron 2DEG, where the renormalized  $m^*$  exceeds the band mass by 40% at  $r_s \sim 5$  due to  $e-e$  interaction [18]. Here, we find that  $m_e^*$  and  $m_h^*$  behave very differently as  $n$  decreases. While  $m_e^*$  continues to follow the high-density TB extrapolation,  $m_h^*$  sharply dives in value below  $n = 6 \times 10^{11} \text{ cm}^{-2}$ , reaching about 70% of the TB band mass at  $n = 2 \times 10^{11} \text{ cm}^{-2}$ . A thorough theoretical investigation evaluating the effect of  $e-e$  interaction in different approximations, together with the effect of Coulomb potential disorder, identifies density

\*Present address: Department of Chemistry, The Makineni Theoretical Laboratories, University of Pennsylvania, Philadelphia, Pennsylvania 19104-6323, USA; Corresponding author: liangtan@sas.upenn.edu

†Present address: Department of Applied Physics, Center for Research on Interface Structures and Phenomena (CRISP), Yale University, New Haven, Connecticut 06520, USA.

‡Corresponding author: sglouie@berkeley.edu

§Corresponding author: jzhu@phys.psu.edu

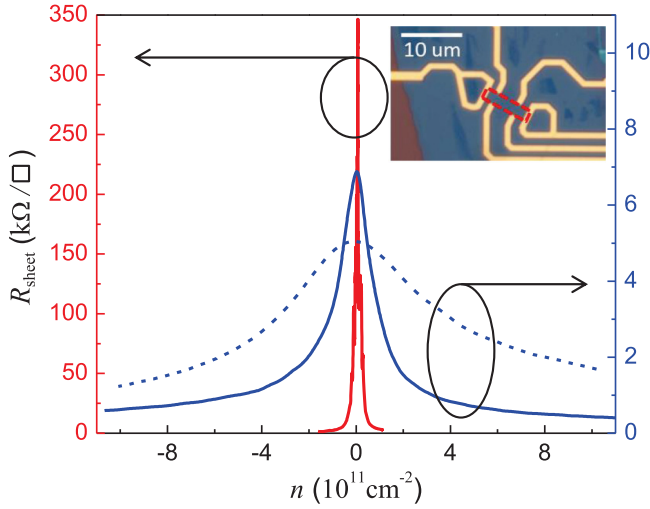


FIG. 1. Sheet resistance vs carrier density  $R_{\text{sheet}}(n)$  for samples A (solid red), B (solid blue), and C (dashed blue). Samples A and B are supported on h-BN; sample C is supported on  $\text{SiO}_2$ . The field effect mobility  $\mu_{\text{FE}}$  is 30 000, 20 000, and 4000  $\text{cm}^2 \text{V}^{-1} \text{s}^{-1}$ , respectively, for samples A–C.  $T = 1.6 \text{ K}$ . The large resistance sample A exhibits at the CNP results from a finite band gap caused by unintentional doping. We discuss the effect of a band gap on the band mass in Fig. S4 of the Supplemental Material [39]. The inset: An optical micrograph for sample A.

inhomogeneity to be a key factor in explaining the experimental observations. This unusual effect of disorder is unique to 2D semimetallic systems.

Bilayer multi-terminal devices are made by exfoliating, transferring, stacking, and patterning of a multi-layer-graphene bottom gate electrode, 15–30-nm-thick h-BN gate dielectric (Sources are PolarTherm grade PT110 from Momentive and The National Institute for Material Science of Japan) and bilayer graphene sheet (Kish Graphite) using a polymethyl-methacrylate-/poly(vinylalcohol-) based transfer method [38] and standard  $e$ -beam lithography. Transport experiments are carried out in a variable-temperature pumped  $\text{He}^4$  cryostat with a 9-T magnet using a standard low-frequency lock-in technique (47 Hz) with a current excitation of 50 nA. Figure 1 plots the sheet resistance vs carrier density  $R_{\text{sheet}}(n)$  of samples A and B, together with sample C reported in Zou *et al.* [10] for comparison. The field effect mobility  $\mu_{\text{FE}}$  is 30 000  $\text{cm}^2 \text{V}^{-1} \text{s}^{-1}$  and 22 000  $\text{cm}^2 \text{V}^{-1} \text{s}^{-1}$ , respectively, in samples A and B, in comparison to  $\mu_{\text{FE}} = 4000 \text{ cm}^2 \text{V}^{-1} \text{s}^{-1}$  in sample C, which is supported on a  $\text{SiO}_2$  substrate. The unintentional doping for both devices are moderate, and the effect of the displacement ( $D$ ) field on the bare band mass is modeled in Sec. S4 of the Supplemental Material for both devices [39]. We find that the presence of a small  $D$  field does not change the conclusions of the paper.

The effective mass  $m^*$  as measured in quantum oscillations is given by

$$m^* = \frac{\hbar^2}{2\pi} \left. \frac{dA(E)}{dE} \right|_{E=E_F}, \quad (1)$$

where  $A(E)$  is the  $k$ -space area enclosed by the contour of constant energy  $E$  in the quasiparticle band structure.

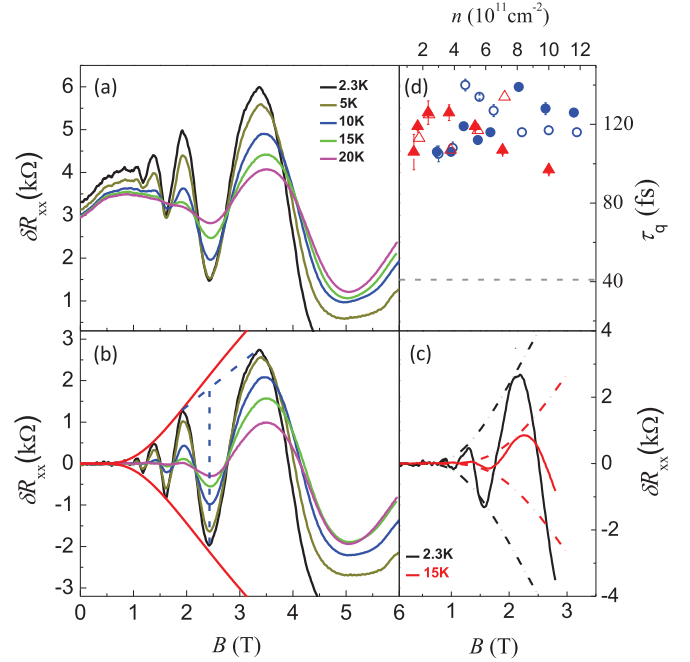


FIG. 2. (a)  $T$ -dependent magnetoresistance  $R_{xx}(B)$  for  $n_h = 4.7 \times 10^{11} \text{ cm}^{-2}$  at selected temperatures as indicated in the plot. (b) Oscillation amplitude  $\delta R_{xx}(B)$  of the data in (a) after background subtraction. The solid red curve plots Eq. (2) with fitting parameters  $m_h^* = 0.0347 m_e$  and  $\tau_q = 140 \text{ fs}$ .  $T = 2.3 \text{ K}$ .  $\delta R_{xx}(B)$  starts deviating from the fit above  $B = 3 \text{ T}$ . The conventional method used to extract  $\delta R_{xx}$  is illustrated by the blue dashed lines and produces  $m^* = 0.0311(2)m_e$ . This is 10% smaller than  $m_h^* = 0.0347 m_e$  obtained from the global fitting. (c)  $\delta R_{xx}(B)$  for  $n_h = 3.0 \times 10^{11} \text{ cm}^{-2}$  at  $T = 2.3$  and  $T = 15 \text{ K}$ . The dashed curves are fits to Eq. (2) with  $m_h^* = 0.0285 m_e$  and  $\tau_q = 107 \text{ fs}$ . Data in (a)–(c) are from sample B. (d) The quantum scattering time  $\tau_q$  as a function of carrier density in sample A (red symbols) and sample B (blue symbols). Electrons are shown by the filled symbols, and holes are shown by the open symbols.  $\tau_q$  is about 40 fs (dashed gray line) in sample C (Ref. [10]).

To accurately determine  $m^*$ , we measure the temperature-dependent magnetoresistance  $R_{xx}(B)$  at a fixed carrier density [Fig. 2(a)], extract the low-field Shubnikov–de Haas (SdH) oscillation amplitude  $\delta R_{xx}(T, B)$  and perform simultaneous fitting of the temperature and magnetic-field dependence to the Lifshitz-Kosevich formula [40],

$$\frac{\delta R_{xx}}{R_0} = 4\gamma_{th} \exp\left(\frac{-\pi}{\omega_c \tau_q}\right), \quad \gamma_{th} = \frac{2\pi^2 k_B T / \hbar \omega_c}{\sinh(2\pi^2 k_B T / \hbar \omega_c)}, \quad (2)$$

where  $\omega_c = \frac{eB}{m^*}$  is the cyclotron frequency. The effective mass  $m^*$  and the quantum scattering time  $\tau_q$  are the two fitting parameters.

This global fitting procedure is illustrated in Figs. 2(b) and 2(c) for two carrier densities  $n_h = 4.7$  and  $3.0 \times 10^{11} \text{ cm}^{-2}$  as examples (see Secs. S1 and S2 of the Supplemental Material [39]). Compared to the common practice of approximating  $\delta R_{xx}$  at a particular  $B$  field by linearly interpolating adjacent peak heights and analyzing its  $T$  dependence to obtain  $m^*$ , fits to Eq. (2) better represent the oscillation amplitude  $\delta R_{xx}$ , especially at low carrier densities

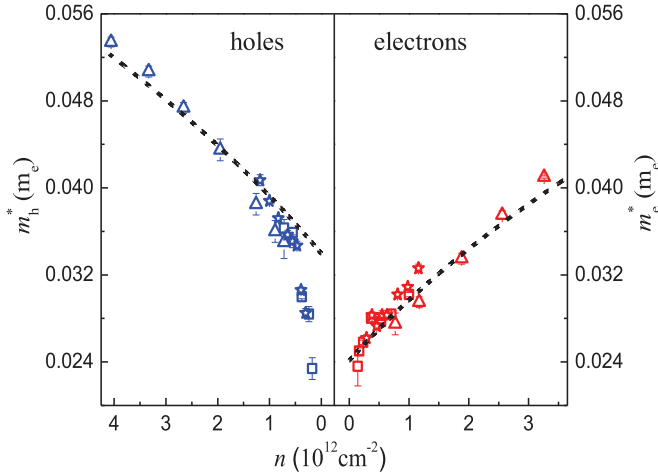


FIG. 3. The effective carrier masses  $m_h^*$  and  $m_e^*$  as a function of the carrier density (red for electrons, blue for holes) in samples A (squares), B (stars), and C (triangles). The data on sample C are from Ref. [10]. Together, the measurement covers the density range of approximately  $1.4\text{--}4.1 \times 10^{11} \text{ cm}^{-2}$ . The dashed curves plot  $m^*$  calculated using a  $4 \times 4$  tight-binding Hamiltonian with hopping parameters  $\gamma_0 = 3.43 \text{ eV}$ ,  $\gamma_1 = 0.40 \text{ eV}$ ,  $\gamma_3 = 0$ , and  $v_4 = 0.063$ . These values are obtained in Ref. [10] by fitting the data in sample C at high densities.

when only a few oscillations are available [see Fig. 2(c), for example]. It also enables us to discern and avoid using the  $T$ -dependent oscillations of nascent quantum Hall states, the analysis of which can lead to errors in  $m^*$  [see the caption in Fig. 2(b)]. The effective mass  $m^*$  obtained using the global fitting procedure is independent of the  $B$  field by virtue of the method and best extrapolates to the density-of-states mass of the bilayer graphene at  $B = 0$ , which is expected to be modified by  $e$ - $e$  interactions [30–35].

The above analysis enables us to accurately determine both the electron and the hole effective mass  $m_h^*$  and  $m_e^*$  for the approximate carrier density range of  $1\text{--}10 \times 10^{11} \text{ cm}^{-2}$ . The uncertainty of  $m^*$  varies from  $\pm 0.0002$  to  $\pm 0.004 m_e$  from high to low densities. The high accuracy of the measurements facilitates comparison to theory as interaction corrections to  $m^*$  are expected to be typically in the few to tens of percent range [16,18]. Also plotted in Fig. 2(d) is the quantum scattering time  $\tau_q$  in both samples.  $\tau_q$  is between 100 and 140 fs for both electrons and holes. Compared to  $\sim 40$  fs in sample C [10], the high values of  $\tau_q$  in samples A and B attest to the improvement of sample quality. Below  $n = 1 \times 10^{11} \text{ cm}^{-2}$ , the SdH oscillations become increasingly more nonsinusoidal due to density inhomogeneity and global fits cannot be obtained reliably.

Figure 3 plots  $m_h^*$  and  $m_e^*$  obtained in samples A and B, together with data from sample C in Ref. [10]. In the overlapping density regime, current and previous results agree very well and are well described by the TB model with hopping parameters  $\gamma_0 = 3.43 \text{ eV}$ ,  $\gamma_1 = 0.40 \text{ eV}$ ,  $\gamma_3 = 0$ ,  $v_4 = \gamma_4/\gamma_0 = 0.063$ , and  $\Delta = 0.018 \text{ eV}$ , which are determined in Ref. [10]. The calculated  $m^*$ 's are plotted as dashed lines in Fig. 3. The electron and hole branches use the same set of parameters with their mass differences captured by  $v_4$ . In current samples, the TB parameters continue to describe all

the  $m_e^*$  data very well down to the lowest density measured. On the hole side, however,  $m_h^*$  exhibits a sharp drop from the TB model as  $n_h$  is decreased to less than  $5 \times 10^{11} \text{ cm}^{-2}$ , reaching a large suppression of 30% at  $n_h = 2 \times 10^{11} \text{ cm}^{-2}$ . These densities are still sufficiently high that the effect of trigonal warping [1] can be safely neglected. (See Fig. S6 of the Supplemental Material [39].)

In existing theoretical studies of bilayer electronic dispersions, the effect of  $e$ - $e$  interaction manifests in two ways, i.e., by renormalizing the hopping parameters within the TB model at high carrier densities [33] and by causing deviations of  $m^*$  from the TB description at low carrier densities. There different trends of  $m^*$  are predicted [30–32,34,35].

We begin our calculations with a four-band TB Hamiltonian with noninteracting hopping parameters and explicitly include the  $e$ - $e$  interaction with the random-phase approximation (RPA) of the screened exchange self-energy,

$$\Sigma(k) = - \sum_q \frac{V^{2D}(q)}{\varepsilon(q)} F^{ss'}(k, k+q), \quad (3)$$

using a dielectric function  $\varepsilon(q) = \varepsilon_{BN} - V^{2D}(q)\chi(q)$ , that includes contributions from both the bilayer graphene and the h-BN substrate and overlayer. Here  $\varepsilon_{BN} = 3.0$  is determined from the gating efficiency of the backgate, and  $F^{ss'}$  is the pseudospin overlap factor [30,31]. Equation (3) provides the RPA correction to the bare energy bands  $E_0(k)$  obtained from TB calculation to yield the quasiparticle band-structure  $E(k) = E_0(k) + \Sigma(k)$ . The effective mass is then computed using Eq. (1).

The calculated  $m_e^*$  and  $m_h^*$  are plotted in Fig. 4 in olive dotted lines. Interaction leads to a slightly faster decrease in  $m_e^*$  and  $m_h^*$  at low carrier densities, in contrast to the sudden drop observed in the measured  $m_h^*$  for  $n_h < 5 \times 10^{11} \text{ cm}^{-2}$ . Examining the problem from a different angle, we note that in the RPA model, the dielectric function is well described by the Thomas-Fermi (TF) screening  $\varepsilon(q) = \varepsilon_{BN} + \frac{q_{TF}}{q}$  in the small  $q$  limit [34]. Fitting the TF description to our data yields a tenfold reduction of the TF screening wave-vector  $q_{TF}$  from its expected value of  $q_{TF} = m^* e^2 / \hbar^2$ . This would imply extremely weak screening of the  $e$ - $e$  interaction in our devices, which cannot be justified. (See Fig. S7 of the Supplemental Material [39].) Thus, the  $e$ - $e$  interaction effect, at least at the RPA level, appears to be too weak to account for the experimental observations. In comparison, in monolayer graphene, a large suppression of  $m^*$  is also observed at low carrier densities and well described by RPA calculations [28].

Can Coulomb potential fluctuation and the resulting density inhomogeneity [36,37,41] play a role? The answer is not so intuitive at the first glance. In a conventional semiconducting 2DEG, density inhomogeneity results in the smearing of  $m^*(n)$ . This effect does not alter the trend of  $m^*(n)$  and is typically nonconsequential in the carrier density regime where the SdH oscillations are well behaved. In Fig. 2(c), the SdH oscillations at  $n_h = 3 \times 10^{11} \text{ cm}^{-2}$  appear to be well behaved, yet the measured  $m_h^*$  is already 14% below the TB band mass. Here, the *gapless* nature of the bilayer bands makes a crucial difference between a bilayer graphene and a conventional 2DEG. As the inset of Fig. 4 illustrates, as the Fermi energy  $E_F$  approaches the disorder energy scale  $\delta E$ ,

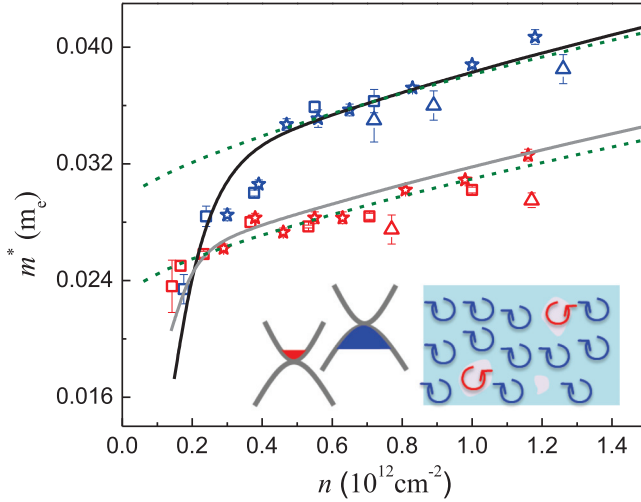


FIG. 4. Comparison of calculations and experiment at low carrier density ( $0.2\text{--}1.3 \times 10^{12} \text{ cm}^{-2}$ ). Experimental data follow the symbols used in Fig. 3. The olive dashed lines plot the calculated  $m^*$  including the  $e\text{--}e$  interaction in a random-phase approximation. The black and gray lines are calculations that further include the effect of potential disorder using  $\delta E = 5.4 \text{ meV}$  obtained from  $\tau_q$  and the temperature dependence of the conductance. In both calculations,  $\gamma_0 = 3.08 \text{ eV}$  and  $\gamma_1 = 0.36 \text{ eV}$  are chosen to fit the experimental data in the high-density regime. Their values differ from those obtained in Ref. [10] since the  $e\text{--}e$  interaction is explicitly calculated here whereas in Ref. [10] its effect is represented by renormalizing the hopping parameters.  $\gamma_3 = 0$  and  $v_4 = 0.063$  are taken from Ref. [10]. The inset: a schematic of the electron-hole coexistence at low carrier densities due to disorder and its effect on the cyclotron motion.

instead of depletion, carriers of the opposite sign start to appear in parts of the sample. The SdH oscillations of a minority carrier type have the opposite sign in  $dA/dE$ ; their presence in some regions of the sample thus contribute negatively to the average of  $m^*$ , resulting in a decrease in its value. Such a cancellation effect does not occur in a conventional semiconductor 2DEG.

This situation can be modeled by defining the overall carrier density and effective mass as ensemble averages of their local counterparts  $n_{\text{loc}}$  and  $m_{\text{loc}}$ , respectively,

$$n(E) = \langle n_{\text{loc}} \rangle = \int d\mu f(\mu) n_{\text{loc}}(E + \mu), \quad (4)$$

$$m(E) = \langle m_{\text{loc}} \rangle = \int d\mu f(\mu) m_{\text{loc}}(E + \mu), \quad (5)$$

Here, the fluctuation of energy is assumed to have a Gaussian profile  $f(\mu)$  with a standard deviation of  $\delta E$ .

Effective masses calculated using the RPA model and including disorder characterized by a broadening energy of  $\delta E = 5.4 \text{ meV}$  are plotted as solid lines in Fig. 4. Evidently, the combination of the  $e\text{--}e$  interaction and Coulomb potential fluctuations can now quantitatively reproduce the observed behavior of  $m_e^*$  and  $m_h^*$  over the entire range of measurement and for both samples. Remarkably, the same value for  $\delta E$  simultaneously captures the sharp decrease in  $m_h^*$  at  $n_h < 5 \times 10^{11} \text{ cm}^{-2}$  and the absence of such a decrease on the electron side. Our calculations predict that  $m_e^*$  should also substantially

decrease from the TB values at yet lower carrier densities, just below the range probed in our measurements. The difference arises from a smaller electron-density inhomogeneity due to a smaller  $m_e^*$ . The quantum scattering time  $\tau_q \sim 120 \text{ fs}$  found in both samples [Fig. 2(d)] yields  $\delta E \sim \hbar/2\tau_q \sim 2.7 \text{ meV}$ , in good agreement with the theoretical fit. In addition, we can estimate the density fluctuation  $\delta n$  by locating the onset density  $n^*$  at which the conductance sharply increases with density [11–15].  $n^*$  is approximately  $2 \times 10^{10} \text{ cm}^{-2}$  in sample A and  $4 \times 10^{10} \text{ cm}^{-2}$  in sample B (see Fig. S4 in the Supplemental Material [39]). These values are also consistent with estimates obtained by locating the crossover density  $n(h/e)_c \sim 5 \times 10^{10} \text{ cm}^{-2}$  where the temperature dependence of  $R(n)$  changes from that of a metal, i.e.,  $dR/dT > 0$  to that of an insulator, i.e.,  $dR/dT < 0$  [42] in a bilayer sample of similar quality. A  $\delta n$  of  $5 \times 10^{10} \text{ cm}^{-2}$  corresponds to  $\delta E = 2 \text{ meV}$  using  $m^* = 0.03 m_e$ . These consistent estimates of disorder energy scales support the fitting value of  $\delta E$  used for both samples. Furthermore, our calculations also show that interaction renormalizes the interband transition energy  $\gamma_1$  from the bare value of  $0.36 \text{ eV}$  (Fig. 4) to  $0.38 \text{ eV}$ , in excellent agreement with infrared absorption measurements [6,7,9].

In Ref. [10], we have shown that a set of renormalized TB hopping parameters can capture  $m^*$  in the high-density regime very well without explicitly including  $e\text{--}e$  interactions (see the dashed lines in Fig. 3). In Fig. S8 of the Supplemental Material [39], we show that adding disorder broadening  $\delta E$  to this set of parameters can also capture the main trend of the data, with the diving of  $m_h^*$  at low densities slightly too abrupt compared to experiment.

The above studies highlight a few remarkable differences between bilayer graphene, a gapless Dirac Fermi liquid, and conventional semiconductor 2DEGs. First, both our calculations and measurements suggest that the effect of the  $e\text{--}e$  interaction on  $m^*$  in bilayer graphene remains weak down to  $n \sim 2 \times 10^{11} \text{ cm}^{-2}$  ( $r_s = 5.3$ ) whereas past studies on GaAs electrons showed an enhancement of more than 40% at this interaction parameter [18]. Second, the effect of disorder appears quite differently in these two systems. In conventional semiconducting 2DEGs, disorder leads to localization and therefore the *increase* rather than the decrease in  $m^*$  at low carrier densities [18]. Here in gapless bilayer graphene, disorder leads to coexisting electrons and holes and consequently a partial cancellation effect on  $m^*$ . In comparison to the well-recognized Klein tunneling effect in  $p\text{--}n$  junctions [43,44], this study exposed a more elusive effect of electron-hole puddles. Studies of low carrier density regimes in Dirac materials thus require a great deal of caution. For now, samples of yet higher qualities are necessary to elucidate the intrinsic behavior of  $m^*$  near the charge neutral point of bilayer graphene.

In conclusion, we have performed careful measurements of the effective mass  $m^*$  in high-quality h-BN-supported bilayer graphene samples down to the carrier density regime of  $1 \times 10^{11} \text{ cm}^{-2}$  and observed a sharp decrease in the hole mass at low carrier densities. Our calculations show that, although the inclusion of electron-electron interaction is necessary to reach excellent quantitative agreement with the data at all carrier densities, Coulomb potential fluctuations, which result

in the coexistence of electron and hole regions and a partial cancellation of  $m^*$ , is chiefly responsible for the observed sharp drop in  $m_h^*$  at low densities. This mechanism, which is absent in finite-gap semiconductor two-dimensional systems, is another manifestation of the unusual consequences of gapless Dirac bands.

J.L., K.Z., A.A.S., D.J.S., and J.Z. are supported by the NSF under Grant No. DMR-1506212 and by the ONR under Grant No. N00014-11-1-0730. L.Z.T. and S.G.L. are supported by the Theory Program at the Lawrence Berkeley National Laboratory through the Office of Basic Energy

Sciences, U.S. Department of Energy under Contract No. DE-AC02-05CH11231 which provided theoretical analyses and simulations of disorder effects and by the National Science Foundation under Grant No. DMR15-1508412 which provided for the calculation of electron-electron interaction effects. K.W. and T.T. are supported by the Elemental Strategy Initiative conducted by the MEXT, Japan. T.T. is also supported by a Grant-in-Aid for Scientific Research on Grant No. 262480621 and on Innovative Areas “Nano Informatics” (Grant No. 25106006) from JSPS. The authors acknowledge the use of facilities at the PSU site of NSF NNIN. We are grateful for helpful discussions with X. Hong.

- 
- [1] M. Edward and K. Mikito, *Rep. Prog. Phys.* **76**, 056503 (2013).  
 [2] M. Mucha-Kruczynski, E. McCann, and V. I. Fal’ko, *Semicond. Sci. Technol.* **25**, 033001 (2010).  
 [3] J. Nilsson, A. H. Castro Neto, F. Guinea, and N. M. R. Peres, *Phys. Rev. B* **78**, 045405 (2008).  
 [4] J. Jung and A. H. MacDonald, *Phys. Rev. B* **89**, 035405 (2014).  
 [5] E. A. Henriksen and J. P. Eisenstein, *Phys. Rev. B* **82**, 041412 (2010).  
 [6] A. B. Kuzmenko, I. Crassee, D. van der Marel, P. Blake, and K. S. Novoselov, *Phys. Rev. B* **80**, 165406 (2009).  
 [7] Z. Q. Li, E. A. Henriksen, Z. Jiang, Z. Hao, M. C. Martin, P. Kim, H. L. Stormer, and D. N. Basov, *Phys. Rev. Lett.* **102**, 037403 (2009).  
 [8] L. M. Malard, J. Nilsson, D. C. Elias, J. C. Brant, F. Plentz, E. S. Alves, A. H. Castro Neto, and M. A. Pimenta, *Phys. Rev. B* **76**, 201401 (2007).  
 [9] L. M. Zhang, Z. Q. Li, D. N. Basov, M. M. Fogler, Z. Hao, and M. C. Martin, *Phys. Rev. B* **78**, 235408 (2008).  
 [10] K. Zou, X. Hong, and J. Zhu, *Phys. Rev. B* **84**, 085408 (2011).  
 [11] P. Maher, C. R. Dean, A. F. Young, T. Taniguchi, K. Watanabe, K. L. Shepard, J. Hone, and P. Kim, *Nat. Phys.* **9**, 154 (2013).  
 [12] J. Velasco, Jr. *et al.*, *Nat. Nanotechnol.* **7**, 156 (2012).  
 [13] A. S. Mayorov *et al.*, *Science* **333**, 860 (2011).  
 [14] R. T. Weitz, M. T. Allen, B. E. Feldman, J. Martin, and A. Yacoby, *Science* **330**, 812 (2010).  
 [15] B. E. Feldman, J. Martin, and A. Yacoby, *Nat. Phys.* **5**, 889 (2009).  
 [16] Y. W. Tan, J. Zhu, H. L. Stormer, L. N. Pfeiffer, K. W. Baldwin, and K. W. West, *Physica E* **34**, 260 (2006).  
 [17] R. Asgari, B. Davoudi, M. Polini, G. F. Giuliani, M. P. Tosi, and G. Vignale, *Phys. Rev. B* **71**, 045323 (2005).  
 [18] Y. W. Tan, J. Zhu, H. L. Stormer, L. N. Pfeiffer, K. W. Baldwin, and K. W. West, *Phys. Rev. Lett.* **94**, 016405 (2005).  
 [19] S. V. Kravchenko and M. P. Sarachik, *Rep. Prog. Phys.* **67**, 1 (2004).  
 [20] V. M. Pudalov, M. E. Gershenson, H. Kojima, N. Butch, E. M. Dizhur, G. Brunthaler, A. Prinz, and G. Bauer, *Phys. Rev. Lett.* **88**, 196404 (2002).  
 [21] Y. K. Kwon, D. M. Ceperley, and R. M. Martin, *Phys. Rev. B* **50**, 1684 (1994).  
 [22] G. Giuliani and G. Vignale, *Quantum Theory of the Electron Liquid* (Cambridge University Press, Cambridge, U.K., 2005).  
 [23] E. H. Hwang and S. Das Sarma, *Phys. Rev. B* **75**, 205418 (2007).  
 [24] M. Polini, R. Asgari, G. Borghi, Y. Barlas, T. Pereg-Barnea, and A. H. MacDonald, *Phys. Rev. B* **77**, 081411 (2008).  
 [25] C.-H. Park, F. Giustino, C. D. Spataru, M. L. Cohen, and S. G. Louie, *Nano Lett.* **9**, 4234 (2009).  
 [26] S. Das Sarma, S. Adam, E. H. Hwang, and E. Rossi, *Rev. Mod. Phys.* **83**, 407 (2011).  
 [27] V. N. Kotov, B. Uchoa, V. M. Pereira, F. Guinea, and A. H. Castro Neto, *Rev. Mod. Phys.* **84**, 1067 (2012).  
 [28] D. C. Elias *et al.*, *Nat. Phys.* **7**, 701 (2011).  
 [29] D. A. Siegel, C.-H. Park, C. Hwang, J. Deslippe, A. V. Fedorov, S. G. Louie, and A. Lanzara, *Proc. Natl. Acad. Sci. USA* **108**, 11365 (2011).  
 [30] A. Sabashvili, S. Ostlund, and M. Granath, *Phys. Rev. B* **88**, 085439 (2013).  
 [31] R. Sensarma, E. H. Hwang, and S. Das Sarma, *Phys. Rev. B* **84**, 041408 (2011).  
 [32] Y. Lemonik, I. L. Aleiner, C. Toke, and V. I. Fal’ko, *Phys. Rev. B* **82**, 201408 (2010).  
 [33] P. Gava, M. Lazzeri, A. M. Saitta, and F. Mauri, *Phys. Rev. B* **79**, 165431 (2009).  
 [34] G. Borghi, M. Polini, R. Asgari, and A. H. MacDonald, *Solid State Commun.* **149**, 1117 (2009).  
 [35] S. V. Kusminskiy, D. K. Campbell, and A. H. Castro Neto, *Europhys. Lett.* **85**, 58005 (2009).  
 [36] K. Zou and J. Zhu, *Phys. Rev. B* **82**, 081407 (2010).  
 [37] A. Deshpande, W. Bao, Z. Zhao, C. N. Lau, and B. J. LeRoy, *Appl. Phys. Lett.* **95**, 243502 (2009).  
 [38] C. R. Dean *et al.*, *Nat. Nanotechnol.* **5**, 722 (2010).  
 [39] See Supplemental Material at <http://link.aps.org/supplemental/10.1103/PhysRevB.94.161406> for more details about the global fitting procedure, estimation of density fluctuation, effects of the band gap, and trigonal warping on  $m^*$  and more theoretical fits.  
 [40] D. Shoenberg, *Magnetic Oscillations in Metals* (Cambridge University Press, Cambridge, U.K., 1984).  
 [41] M. Yankowitz, J. Xue, and B. J. LeRoy, *J. Phys.: Condens. Matter* **26**, 303201 (2014).  
 [42] C. Cobaleda, S. Pezzini, E. Diez, and V. Bellani, *Phys. Rev. B* **89**, 121404 (2014).  
 [43] A. F. Young and P. Kim, *Annu. Rev. Condens. Matter Phys.* **2**, 101 (2011).  
 [44] V. V. Cheianov and V. I. Fal’ko, *Phys. Rev. B* **74**, 041403 (2006).